Optical properties of InGaAsBi/GaAs strained quantum wells studied by temperature-dependent photoluminescence*

Gu Yi(顾 溢)[a], Zhang Yong-Gang(张永刚)[a]†, Song Yu-Xin(宋禹忻)[b], Ye Hong(叶 虹)[b], Cao Yuan-Ying(曹远迎)[a], Li Ai-Zhen(李爱珍)[a], and Wang Shu-Min(王庶民)[a,b]

[a] *State Key Laboratory of Functional Materials for Informatics, Shanghai Institute of Microsystem and Information Technology, Chinese Academy of Sciences, Shanghai* 200050, *China*

[b] *Department of Microtechnology and Nanoscience, Chalmers University of Technology, Gothenburg SE*-41296, *Sweden*

(Received 21 August 2012; revised manuscript received 26 November 2012)

The effect of bismuth on the optical properties of InGaAsBi/GaAs quantum well structures is investigated using the temperature-dependent photoluminescence from 12 K to 450 K. The incorporation of bismuth in the InGaAsBi quantum well is confirmed and found to result in a red shift of photoluminescence wavelength of 27.3 meV at 300 K. The photoluminescence intensity is significantly enhanced by about 50 times at 12 K with respect to that of the InGaAs quantum well due to the surfactant effect of bismuth. The temperature-dependent integrated photoluminescence intensities of the two samples reveal different behaviors related to various non-radiative recombination processes. The incorporation of bismuth also induces alloy non-uniformity in the quantum well, leading to an increased photoluminescence linewidth.

Keywords: InGaAsBi, strained quantum wells, photoluminescence

PACS: 78.55.Cr, 78.67.De, 61.05.cp, 81.15.Hi **DOI:** 10.1088/1674-1056/22/3/037802

1. Introduction

Bismuth (Bi) containing alloys have aroused much attention due to many specific characteristics. The III–V bismides show a strong band-gap dependence on Bi-content, which makes them very promising for the application of long-wavelength optoelectronic devices.[1] Besides, it has been discovered that the band gap and the refractive index of GaAsBi are less temperature sensitive than those of GaAs, and the insensitivity increases with the increasing Bi concentration, an important advantage for the practical realization of cooler-free lasers.[2] Furthermore, unlike the case of dilute nitrides, the bismuth incorporation has a major effect on the valence band and little influence on the conduction band. Due to their heavy atomic masses, the bismides possess a large spin–orbit (SO) split energy, which reduces the Auger recombination and is expected to significantly reduce the threshold current of long wavelength lasers at elevated temperatures.[3] The majority of past work on bismides focused on GaAsBi alloys,[1–3] and there were also sporadic reports on InSbBi,[4] GaSbBi,[5] and InAsBi[6] alloys. A few results have been reported on the growth and characterization of quaternary InGaAsBi bulk on InP substrates.[7,8] A red shift of about 56 meV/% Bi in the optical absorption edge of InGaAsBi was observed by Petropoulos *et al*.[9] In the past decades, much effort has been devoted to realizing uncooled 1.3 μm laser diodes on GaAs substrates using GaInNAs quantum wells (QWs) or InAs quantum dots as the gain medium. The highly strained InGaAs/GaAs QW laser is limited by the critical thickness and can only achieve lasing at wavelengths up to 1.24 μm at room temperature.[10,11] The incorporation of N can effectively reduce the band gap, but at the same time it also causes severe optical degradation due to the N-related non-radiative defects, leading to a high threshold current density.[12,13] The incorporation of Bi into InGaAs/GaAs QWs has the potential to achieve 1.3 μm light emission, and the surfactant effect of using Bi during the growth of III–Vs can reduce the deleterious effect of the non-radiative recombination defects.[14,15] However, the incorporation of Bi into QWs is more complicated than that into bulk alloys. In this work, we investigate the optical properties of InGaAsBi/GaAs QWs on GaAs substrates by using temperature dependent photoluminescence (PL), and we compare it with the strained InGaAs QW. The incorporation of Bi in the QW significantly enhances the PL intensity and red-shifts the emission wavelength, but does not improve the temperature sensitivity of the band gap at about 0.6% Bi content.

2. Experiments

All the samples were grown on (001)-oriented semi-insulating GaAs substrates using a Riber Compact21 solid source molecular beam epitaxy system. As shown in the inset of Fig. 1, the growth of InGaAsBi QW samples started with a 50-nm-thick GaAs buffer followed by a 100-nm-thick $Al_{0.2}Ga_{0.8}As$ layer grown at 580 °C. Then the growth tem-

*Project supported by the National Basic Research Program of China (Grant No. 2012CB619200), the National Natural Science Foundation of China (Grant Nos. 61275113, 61204133, and 60906047), the Innovative Founding of Shanghai Institute of Microsystem and Information Technology, Chinese Academy of Sciences, and the Swedish Research Council.

†Corresponding author. E-mail: ygzhang@mail.sim.ac.cn

© 2013 Chinese Physical Society and IOP Publishing Ltd

perature was decreased to 370 °C (thermocouple temperature) to enhance the incorporation of Bi in the QW, and a 7.5-nm-thick InGaAsBi QW layer was sandwiched between two 100-nm-thick GaAs barrier layers. Finally, a 100-nm-thick $Al_{0.2}Ga_{0.8}As$ and a 10-nm-thick GaAs cap layer were grown at 580 °C. As a reference, an InGaAs/GaAs QW sample was also grown, differing only in that there was no Bi in the QW layer.

The structural properties of the samples were investigated by the measurements of (004) $\omega/2\theta$ scans using a Philips X'pert MRD high resolution X-ray diffractometer (HRXRD) equipped with a four-crystal Ge (220) monochromator. The PL spectra were measured by using a Nicolet Megna 860 Fourier transform infrared (FTIR) spectrometer, in which an InGaAs detector and a CaF_2 beam splitter were used. A diode-pumped solid-state (DPSS) laser ($\lambda = 532$ nm) was used as the excitation source. The sample was mounted into an Oxford Optistat cryostat for the measurement from 77 K to 450 K and in a continuous-flow helium cryostat from 12 K to 77 K. The PL intensities from 12 K to 77 K were then converted consistently with the intensities from 77 K to 450 K. The detailed PL approach can be found in a previous report.[16] Three different FTIR modes, i.e., rapid scan, double modulation, and step scan, can be switched by software. As the PL signals of those QW samples have relatively strong PL signals with respect to the background, the rapid scan mode was used in the measurements.

3. Results and discussion

The elemental compositions in the QW samples were determined by the HRXRD (004) $\omega/2\theta$ curves shown in Fig. 1. In each curve, the relatively narrow and strong peak comes from the GaAs substrate as well as GaAs and AlGaAs epitaxial layers, while the broad and weak peak corresponds to the strained InGaAs or InGaAsBi QW. The curves have been moved horizontally to place the GaAs peak at standard 30.02° and vertically for distinct observation. It is obvious that the signal of the InGaAsBi QW shifts to a lower angle with respect to that of the InGaAs QW, indicating the higher lattice constant of the InGaAsBi QW. The HRXRD intensities of the layer peaks are relatively weak, implying that the samples may be partly relaxed. Nevertheless, a streaky pattern was observed in the *in-situ* reflection high-energy electron diffraction (RHEED) investigation during the QW growth, and two satellite peaks at around 31° and 32° can be seen in the measured HRXRD curves for the two samples, indicating that the quality of both the QW and the interface is still pretty good. Figure 1 also shows the simulated curves of the two samples assuming that the QW samples are fully strained and the QW thicknesses are 7.5 nm. By careful simulation, the indium composition of 42.6%±0.5% in the InGaAs QW is obtained, and the corresponding bismuth composition in the InGaAsBi QW can be calculated to be about 0.6%. In the calculation, Vegard's law and the lattice constants of 5.653 Å, 6.058 Å, 6.234 Å, and 6.639 Å for GaAs, InAs, GaBi and InBi respectively are used.[7]

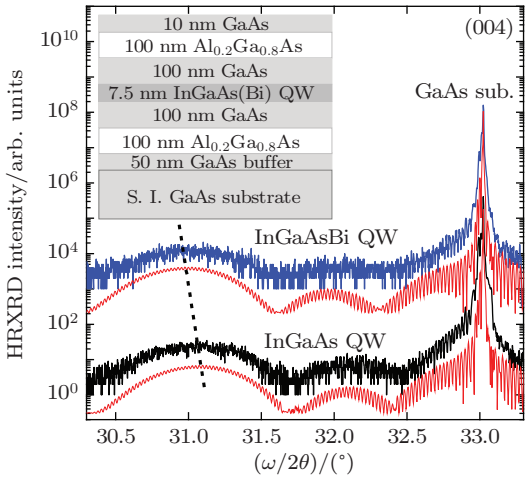


Fig. 1. (color online) HRXRD (004) $\omega/2\theta$ scan curves of the InGaAs and the InGaAsBi QW samples. The red lines are the simulated curves of samples. The inset shows the schematic structure of the samples.

The temperature-dependent PL spectra were carefully measured from 12 K to 450 K and shown in Fig. 2. For each sample at a specific temperature, only one PL peak is observed. Figure 3 shows the PL peak energy and the full width at half maximum (FWHM) each as a function of temperature for the two samples. It can be seen that the PL peak wavelength of the InGaAsBi QW is longer than that of the InGaAs QW. At 300 K, the PL wavelength is red-shifted from 1.21 μm for the InGaAs QW to 1.24 μm for the InGaAsBi QW due to the incorporation of Bi. The red shift of 27.3 meV reveals a Bi content of roughly 0.49%, assuming 56 meV/% Bi for InGaAsBi bulk as obtained in the optical absorption edge investigation[9] and without correcting any difference in the quantum confinement effect between the InGaAs and the InGaAsBi QWs. This is close to the 0.6% estimated from HRXRD and thus confirms the Bi incorporation. The temperature-dependent PL peak energies of the two samples show quite similar behavior in the whole temperature range from 12 K to 450 K. The expected temperature-insensitive behavior of the Bi-containing QW has not been observed, which could be due to the small incorporation of Bi. The solid lines in Fig. 3 are the curves fitted to the experimental results by using the empirical Varshni equation[17]

$$E_g(T) = E_g(0) - \frac{\beta T^2}{\theta_T + T}, \tag{1}$$

where $E_g(0)$ is the 1e-1hh recombination energy at $T = 0$ K, β is the damping constant, and θ_T is the Debye temperature. The

best fitting yields $E_g(0) = 1.102$ eV, $\beta = 0.00047$, $\theta_T = 244$ K for the InGaAs QW; and $E_g(0) = 1.074$ eV, $\beta = 0.00049$, $\theta_T = 274$ K for the InGaAsBi QW. Usually, a deviation of experimental results from the Varshni fitting data at the low temperature can be observed in the PL of QW samples, resulting mainly from the localization of excitons induced by the defects and the alloy composition fluctuation in the QW.[18,19] Here, the deviations are no more than 2 meV for both samples.

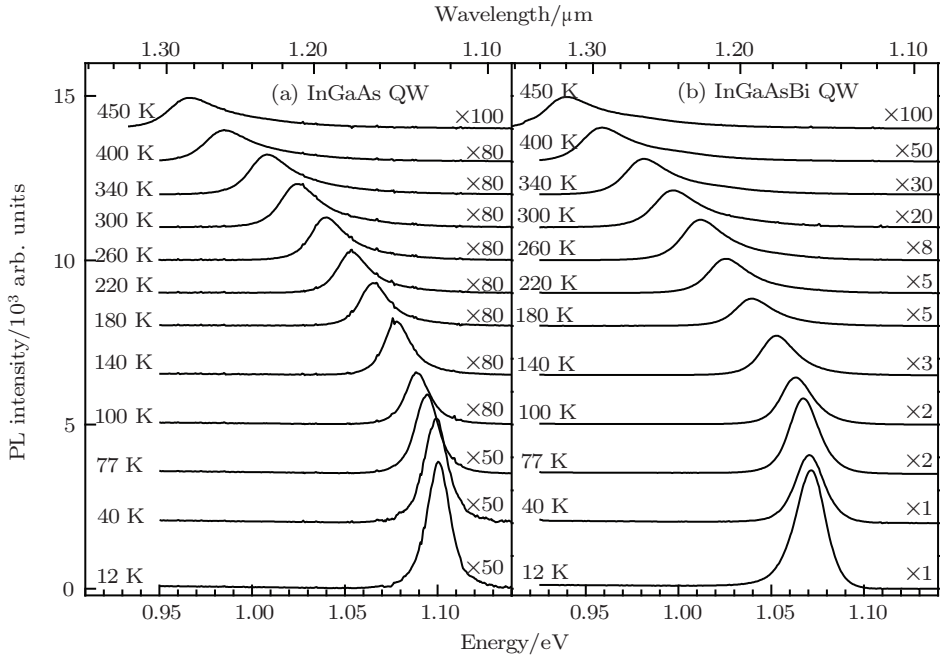


Fig. 2. PL spectra of (a) InGaAs and (b) InGaAsBi QW samples from 12 K to 450 K.

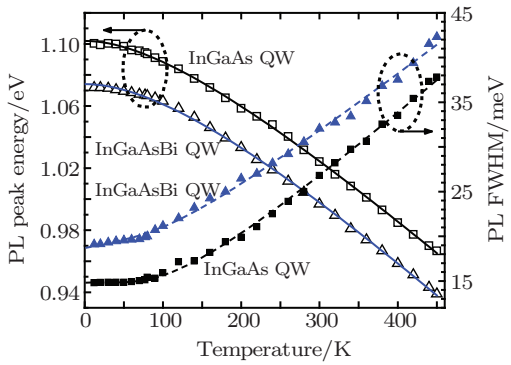


Fig. 3. (color online) Temperature-dependent PL peak energies and FWHMs of InGaAs and InGaAsBi QWs. The solid lines are the best fit to the data using the Varshni equation. The dashed lines are the best fit to the data with Eq. (2) for PL FWHM.

The FWHM of the PL peak can be classified into an inhomogeneous part and a temperature-dependent homogenous part. The inhomogeneous part for the QW is mainly due to the fluctuations of the well width and the alloy compositions, and the interface roughness.[20] Generally, the homogeneous part is mainly attributed to the scattering between phonons and excitons. The temperature dependence of the FWHM can be described by the exciton–phonon coupling model[19]

$$\Gamma(T) = \Gamma_i + \Gamma_{LA} T + \frac{\Gamma_{LO}}{\exp(E_{LO}/k_B T) - 1}, \qquad (2)$$

where Γ_i is the inhomogeneous part, Γ_{LA} and Γ_{LO} represent the coupling strengths of exciton–acoustic phonons and exciton–longitudinal optical (LO) phonons, respectively, E_{LO} is the energy of the LO phonons, and k_B is the Boltzmann constant. The best fittings are shown in Fig. 3 by dashed lines and yield $\Gamma_i = 14.8$ meV, $\Gamma_{LA} = 0.0005$ meV/K, $\Gamma_{LO} = 27.5$ meV for the InGaAs QW, and $\Gamma_i = 18.7$ meV, Γ_{LA}=0.019 meV/K, $\Gamma_{LO} = 17.6$ meV for the InGaAsBi QW. The temperature-independent inhomogeneous part Γ_i of the InGaAsBi QW is larger than that of the InGaAs QW, this may be caused by the Bi-induced non-uniformity and the compositional fluctuation in the QW layer. The coupling strength of exciton–acoustic phonons can be ignored for the InGaAs QW. Although it is enhanced by 38 times for the InGaAsBi QW, it still contributes only 5.7 meV at 300 K. For the InGaAs QW, the Γ_{LO} of 27.5 meV is relatively large and contributes significantly to the linewidth of 12 meV at 300 K. On the other hand, Γ_{LO} is reduced to 17.6 meV for the InGaAsBi QW, and its contribution to the linewidth at 300 K is 7.7 meV, which implies that fewer excitons have been ionized for the InGaAsBi QW.

The non-radiative recombination mechanisms have been investigated based on the temperature-dependent integrated PL intensity. The PL intensities of the two QW samples are plotted in Fig. 4 as a function of the reciprocal temperature, and the integrated intensities are normalized to the integrated PL intensity of the InGaAsBi QW at 12 K. The PL intensity

of the InGaAsBi QW is markedly enhanced, nearly 50 times with respect to that of the InGaAs QW at 12 K, and about 4 times at 300 K. The enhanced PL intensity is probably caused by the surfactant effect of Bi. The lines in Fig. 4 are the fit to the experimental data, following the Arrhenius behavior. For the InGaAs QW, the integrated PL intensity decreases to about 35% as the temperature is increased from 12 K to 180 K, whereas it remains nearly the same from 180 K to 300 K, and decreases only to half when the temperature is increased from 300 K to 450 K. Therefore, the Arrhenius model involving two non-radiative recombination processes should be adopted[18]

$$I(T) = \frac{\alpha}{1 + C_1 \exp(-E_1/k_B T) + C_2 \exp(-E_2/k_B T)}, \quad (3)$$

where T is the measured temperature, $I(T)$ is the PL emission intensity, α is a variable constant, C_1 and C_2 are the ratios of non-radiative to radiative recombination probabilities, while E_1 and E_2 are the thermal activation energies for the two loss mechanisms, respectively. The best fit yields $E_1 = 16.2$ meV and $E_2 = 285$ meV. The non-radiative recombination process with activation energy $E_1 = 16.2$ meV is dominant in the low-temperature range, which could be due to the thermal ionization of excitons from localized states.[21] As the excitons acquire enough thermal energy to escape, they have more possibility to be trapped by the defects and recombine non-radiatively. In the high-temperature range, the non-radiative recombination process with $E_2 = 285$ meV dominates, which is mainly due to the enhancement of the thermal escape of carriers from higher energy sub-bands as the temperature increases.

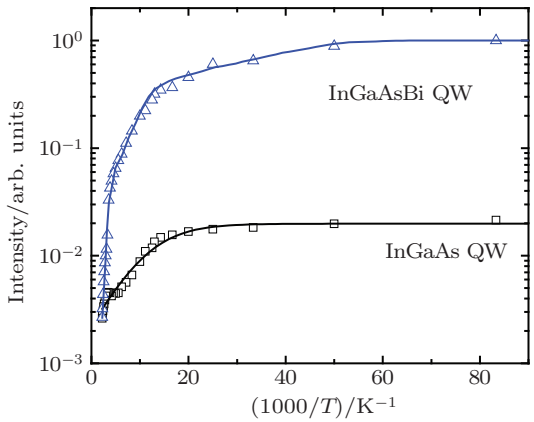


Fig. 4. (color online) Temperature-dependent integrated PL intensities of the InGaAs and the InGaAsBi QWs. The solid lines are the best fit to data with Eq. (3) for the InGaAs QW and Eq. (4) for the InGaAsBi QW.

For the InGaAsBi QW, the Arrhenius model involving only one non-radiative recombination process can match the experimental data well in the whole temperature range

$$I(T) = \frac{\alpha}{1 + C \exp(-E/k_B T)}. \quad (4)$$

The activation energy of $E_a = 175$ meV can be obtained from the fitting. The activation energy $E_1 = 16.2$ meV for the InGaAs QW in the low-temperature range no longer exists for the InGaAsBi QW, suggesting that there is less possibility for the excitons to be thermally ionized and trapped by the defects as the temperature increases after introducing Bi in the QW layer.

4. Conclusion

In conclusion, InGaAsBi and InGaAs strained QW structures have been grown by molecular beam epitaxy and investigated by temperature-dependent PL measurements from 12 K to 450 K. The Bi incorporation in the QW and its composition are determined by X-ray diffraction and further confirmed by the red shift of the PL wavelength. The surfactant effect of Bi significantly enhances the PL intensity about 50 times at 12 K and leads to a constant activation energy in the whole temperature range. The temperature-dependent integrated PL intensities of the two samples reveal different behaviors related to various non-radiative recombination processes. On the other hand, the introduction of Bi also induces alloy non-uniformity in the QW layer, which results in an increased PL FWHM.

References

[1] Francoeur S, Seong M J, Mascarenhas A, Tixier S, Adamcyk M and Tiedje T 2003 *Appl. Phys. Lett.* **82** 3874
[2] Yoshida J, Kita T, Wada O and Oe K 2003 *Jpn. J. Appl. Phys.* **42** 371
[3] Alberi K, Dubon O D, Walukiewicz W, Yu K M, Bertulis K and Krotkus A 2007 *Appl. Phys. Lett.* **91** 051909
[4] Lee J J, Kim J D and Razeghi M 1998 *Appl. Phys. Lett.* **73** 602
[5] Song Y X, Wang S M, Roy I S, Shi P X and Hallen A 2012 *J. Vac. Sci. Technol. B* **30** 02B114
[6] Svensson S P, Hier H, Sarney W L, Donetsky D, Wang D and Belenky G 2012 *J. Vac. Sci. Technol. B* **30** 02B109
[7] Feng G, Yoshimoto M, Oe K, Chayahara A and Horino Y 2005 *Jpn. J. Appl. Phys.* **44** L1161
[8] Zhong Y, Dongmo P B, Petropoulos J P and Zide J M O 2012 *Appl. Phys. Lett.* **100** 112110
[9] Petropoulos J P, Zhong Y and Zide J M O 2011 *Appl. Phys. Lett.* **99** 031110
[10] Sung L W and Lin H H 2003 *Appl. Phys. Lett.* **83** 1107
[11] Chen W C, Su Y K, Chuang R W, Yu H C, Tsai M C, Cheng K Y, Horng J B, Hu C and Tsau S 2008 *IEEE Photon. Technol. Lett.* **20** 264
[12] Wei Y Q, Sadeghi M, Wang S M, Modh P and Larsson A 2005 *Electron. Lett.* **41** 1328
[13] Zhao H, Adolfsson G, Wang S M, Sadeghi M and Larsson A 2008 *Electron. Lett.* **44** 416
[14] Ptak A J, Beaton D A and Mascarenhas A 2012 *J. Cryst. Growth* **351** 122
[15] Naceur H B, Mzoughi T, Moussa I, Nguyen L, Rebey A and Jani B E 2010 *Physica E* **43** 106
[16] Zhang Y G, Gu Y, Wang K, Fang X, Li A Z and Liu K H 2012 *Rev. Sci. Instrum.* **83** 053106
[17] Varshni Y P 1967 *Physica* **34** 149
[18] Shen W Z, Shen S C, Tang W G, Zhao Y and Li A Z 1995 *J. Appl. Phys.* **78** 5696
[19] Lei H P, Wu H Z, Lao Y F, Qi M, Li A Z and Shen W Z 2003 *J. Cryst. Growth.* **256** 96
[20] Gu Y, Zhang Y G, Li A Z, Wang K, Li C and Li Y Y 2009 *Chin. Phys. Lett.* **26** 077808
[21] Sun H D, Calvez S, Dawson M D, Gupta J A, Aers G C and Sproule G I 2006 *Appl. Phys. Lett.* **89** 101909